J. Electrochem. Sci. Eng. **12(5)** (2022) 877-888; http://dx.doi.org/10.5599/jese.1228

Open Access : : ISSN 1847-9286
www.jESE-online.org

Original scientific paper

Microstructural and mechanical properties of CNT-reinforced ZrO_2-Y_2O_3 coated boiler tube steel T-91

Sandeep Kumar[1,✉], Rakesh Bhatia[2], Hazoor Singh[2] and Roshan Lal Virdi[3]

[1]*Department of Mechanical Engineering, Guru Kashi University, Bathinda, Punjab, India*
[2]*Yadavindra Department of Engineering, Punjabi University Guru Kashi Campus, Damdama Sahib, India*
[3]*Department of Mechanical Engineering, Punjabi University, Patiala, India Full Affiliation, Address*

Corresponding author: ✉*sandeep_ycoe@yahoo.com; Tel.:+91-9041021227*

Received: January 1, 2022; Accepted: May 24, 2022; Published: July 26, 2022

Abstract

The main purpose of this study was to fabricate carbon nanotubes (CNTs) reinforced zirconnium yttrium coatings on boiler tube steel and to investigate the microstructural and mechanical properties of these coatings. Plasma sprayed conventional ZrO_2-Y_2O_3, ZrO_2-Y_2O_3 and 1 wt.% CNT and ZrO_2-Y_2O_3 and 4 wt.% CNT were prepared and deposited successfully on boiler tube steel material T-91 (ASTM SA-213) by plasma thermal spray technology. Microhardness, porosity, XRD (X-ray diffraction), SEM/EDAX (scanning electron microscopy/energy dispersive X-ray spectroscopy), X-ray mapping and cross-sectional analyses were used to analyse the specimens. The hardness of CNT reinforced ZrO_2-Y_2O_3 increased with the increase in the percentage of CNT, whereas the porosity of the composite coatings decreased with the increase in the CNT percentage. The observed increase in hardness may be attributed to the content of CNT in the composite coating. The present research gives important information related to the fabrication and physical characteristics of CNT-reinforced ZrO_2-Y_2O_3 coatings deposited on T-91 boiler tube steel.

Keywords

Carbon nanotubes, plasma spray, porosity, hardness

Introduction

In recent years, the importance of stainless steel alloys has attracted considerable attention because of their usage in a wide range of industrial applications to withstand high temperatures and a critical environment. Stainless steel is used to perform in harsh environments, and this seems to be possible due to its excellent mechanical and thermal properties [1]. Serious and never-ending hot corrosion problem occurs in boiler tubes, I.C. engines, power generation equipment, aircraft and gas turbines [2]. In these installations, corrosive salts are formed by low-quality fuels used, which contain Na and V as impurities that can form Na_2SO_4 and V_2O_5 corrosive elements [3]. To

enhance the corrosion resistance of the conventional steels used in thermal power plants, the researchers have applied many types of coatings on these steels.

Thermal spraying methods are one of the important methods of applying coatings on steel to increase its life span [4]. Along with alloys, some reinforced coatings are employed to increase the resistance of the component against high-temperature oxidation [5]. In the recent past, there have been advancements in powder production technologies along with advancements in spraying methods, which have resulted in developing coatings with high corrosion resistance properties [6]. The spraying techniques do not limit the material selection in respect of coatings and substrate composition [7]. These techniques can apply coatings of a few millimeter thicknesses on the steel surface with high hardness. The flame spray, arc spray, plasma and HVOF techniques are used to apply coatings on the boiler components [8,9]. Defect-free plasma coatings are not possible because thermal spray coatings consist of pores and voids. These pores and voids originate at the splat boundaries during the spraying process. Therefore, through these pores and voids, the corrosive elements penetrate towards the substrate material in the corrosive environment [10,11].

The carbon nanotubes (CNTs) were developed and invented by Iijima [12]. The carbon nanotubes have high strength and excellent thermal properties [13–16]. Carbon nanotubes have more than five times elastic constant and more than 100 times tensile strength than conventional steels [17,18]. Due to these properties, CNTs are used as prospective reinforcement for fabricating composite materials [19]. A few researchers have used CNT-metal composite coatings to enhance the corrosion resistance of Ni- and Zn-based composite coatings [20]. CNT reinforced coatings act as an inert physical barrier to initiating and developing corrosion mechanisms. It is revealed in the literature that very few research has been conducted on the corrosion behavior of CNT reinforced coatings. Some researchers have developed different CNTs-Al_2O_3 composite coatings to study their tribological behavior [21-25], but no studies on CNT - zirconium yttrium (ZrO_2-Y_2O_3) composite coatings for high-temperature corrosion are available.

In the present research work, plasma sprayed conventional ZrO_2-Y_2O_3, ZrO_2-Y_2O_3 and 1 wt.% CNT and ZrO_2-Y_2O_3 and 4 wt.% CNT coatings were deposited successfully, as coatings, on T-91 boiler tube steel material to protect in the high-temperature applications.

Experimental

Substrate material

The fresh T-91 boiler tubes were procured from Talwandi Sabo Thermal Power Plant situated at Banawali, Bathinda, Punjab, India. The chemical composition of the base material analyzed using spectroscopy is shown in Table 1. The specimens of 22×15×3 mm were cut from boiler tubes. The standard metallurgical procedures were followed to prepare the samples. Due care was taken to avoid structural and metallurgical changes in the samples. The specimens were then polished using silicon carbide paper. Before deposition of different coatings, the specimens were shot blasted using grit 45 alumina powder.

Table 1. *Chemical composition of T-91*

Composition	Content, wt.%									
	C	Si	Mn	P	S	Cr	Mo	Ni	V	Fe
Nominal	0.07~0.14	0.20~0.50	0.30~0.60	≤0.02	≤0.02	8-9.5	0.85-1.05	0.4	≤0.4	Bal.
Actual	0.12	0.42	0.42	0.016	0.004	8.354	0.93	0.2	0.05	Bal.

Coating powders

Compositions of coating powders were prepared by blending conventional zirconium yttrium, ZrO_2-Y_2O_3 and 1 wt.% CNT, and ZrO_2-Y_2O_3 and 4 wt.% CNT in a laboratory ball mill, using a low-energy ball milling method. Mixing of coating powders was done in a ball mill for 4 hours at 200 rpm [26]. Powder particles were asymmetric in shape and size 45 ± 10 µm. The SEM images of coating powders after mixing in a ball mill are shown in Figures 1 (a)-(c).

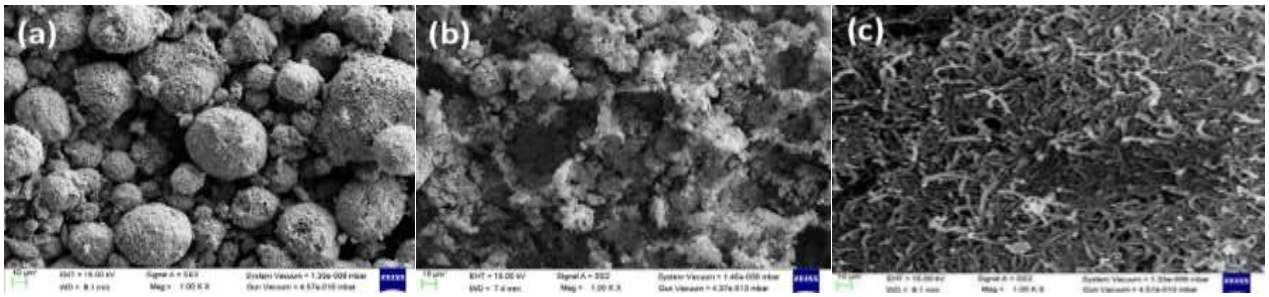

Figure 1. *SEM micrographs of powders of (a) conventional ZrO_2-Y_2O_3; (b) ZrO_2-Y_2O_3 and 1 wt.% CNT and (c) ZrO_2-Y_2O_3 and 4 wt.% CNT*

Formulation of coating

The different CNT mixed ZrO_2-Y_2O_3 coatings were deposited on T-91 boiler steel substrates with a plasma spray process at Metallizing Equipment Company Pvt. Limited, Jodhpur, India. The process parameters selected for the plasma spray technique are shown in Table 2. The process parameters were constant during the deposition of coatings. Coatings of around 250-270 µm thickness were deposited by the plasma spray process. The macrographs of as-coated samples are shown in Figure 2.

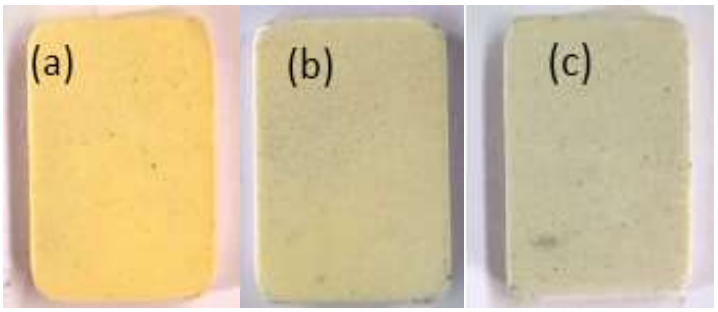

Figure 2. *Macrographs of (a) conventional ZrO_2-Y_2O_3; (b) ZrO_2-Y_2O_3 and 1 wt.% CNT; and (c) ZrO_2-Y_2O_3 and 4 wt.% CNT-coated steel specimen*

Table 2. *Plasma spraying process parameters*

Voltage, V	Current, A	Primary gas (Argon) flow, L min^{-1}	Powder feed rate, g min^{-1}	Spray distance, cm
70	575	39	30	10.16

Coating examinations

The coated specimens were sectioned by a slow-speed diamond cutter at a controlled rate and then hot mounted in epoxy for cross-sectional examination. The mounted specimens were then polished by a standard polishing procedure for XRD, SEM/EDAX and cross-sectional elemental analysis. The microhardness of coated samples was measured from the coating substrate interface [27,28]. The thickness of ZrO_2-Y_2O_3 CNT coated steel specimens was measured with the help of minitest 2000 thin film thickness gauge (Make: Elektro Physik Koln Company, Germany, precision ±1 µm). The image analysis method was adopted to measure the porosity of all the coated

specimens. A PMP3 inverted metallurgical microscope installed with LEICA image analyser software was used to measure the porosity of air plasma sprayed CNT-reinforced zirconium yttrium coatings on T-91 steel specimens. The porosity was evaluated of as-coated samples after polishing by a computer-based analyzing system.

Results

Coating thickness measurement

The thickness of the coating was examined along the cross-section of the specimens. The thickness was found to be in the range of 225-250 µm and is reported in Table 4. The coating thickness was found to be in parity with research work reported in the literature [16,29,30].

Porosity analysis

The thermal spray coatings are generally porous in nature due to splats and voids during deposition. The porosity strongly influences the properties of coatings [26,31]. It is concluded from the literature study that the lower the value of porosity better the corrosion resistance [32,33]. Table 3 shows the porosity values of conventional ZrO_2-Y_2O_3 and ZrO_2-Y_2O_3-CNT coated T-91 steel specimens. The tabulated values clearly show that with the increase in CNT's percentage in ZrO_2-Y_2O_3, the porosity of the coatings decreases. The porosity was evaluated within the range of 3.45 to 4.25 % for the coatings under study. The specimen with ZrO_2-Y_2O_3 and 4 wt.% CNT showed the lowest value of porosity among various coatings under investigation.

Table 3. *Average coating thickness and porosity of different coatings*

Substrate	Coating type	Coating thickness, µm	Porosity, %
ASTM SA-213 T-91	ZrO_2-Y_2O_3	252	4.25
	ZrO_2-Y_2O_3 and 1 wt,% CNT	254	3.62
	ZrO_2-Y_2O_3 and 4 wt,% CNT	247	3.45

Microhardness measurement

Figure 3 shows the microhardness profiles across the cross-section of conventional ZrO_2-Y_2O_3 and CNT coated samples. The microhardness measurement for conventional ZrO_2-Y_2O_3, 99 wt.% ZrO_2-Y_2O_3 and 1 wt.% CNT, and 96 wt.% ZrO_2-Y_2O_3 and 4 wt.% CNT coated specimens were in the range of 789-796, 908-910 and 1047-1051 Hv, respectively.

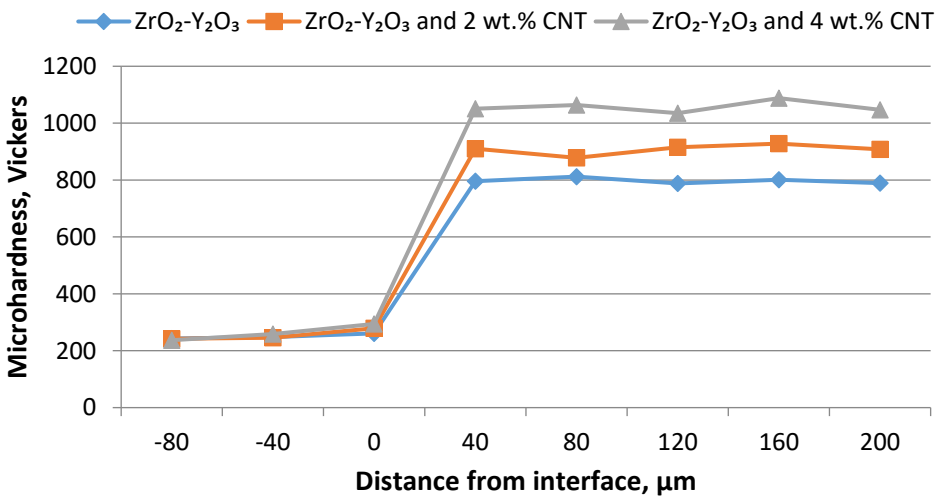

Figure 3. *Microhardness of CNT- ZrO_2-Y_2O_3 reinforced coatings across the cross-section*

It is observed clearly from Figure 3 that with the increase in CNT content in the ZrO_2-Y_2O_3 matrix, the microhardness value of the coating increases. The graph shows the hardness profile along the cross-section of the substrate coating interface and hardness was found uniform across the surface of specimens.

X-ray diffraction analysis

The X-ray diffractions analysis for the surface of CNT- ZrO_2-Y_2O_3 coated specimens was done at IIT Roorkee. The diffraction patterns are shown in Figures 4(a)-(c). The XRD curves of plasma-sprayed ZrO_2-Y_2O_3 coated T-91 boiler tube steel sample showed ZrO_2-Y_2O_3 as the main phase present during analysis. The XRD peaks of ZrO_2-Y_2O_3 and 1 wt.% CNT and ZrO_2-Y_2O_3 and 4 wt.% CNT composite coating also depicted ZrO_2-Y_2O_3 as the main phase with a small proportion of carbon, as shown in Figure 4(b). C peaks indicate the presence of CNT content in the coating matrix peaks increased with an increase in CNT percentage, as shown in Figure 4(c). The C peaks in the diffraction pattern indicated that the CNTs were present in the pure carbon form in the coating matrix and had not reacted with ZrO_2-Y_2O_3 to form any complex compounds.

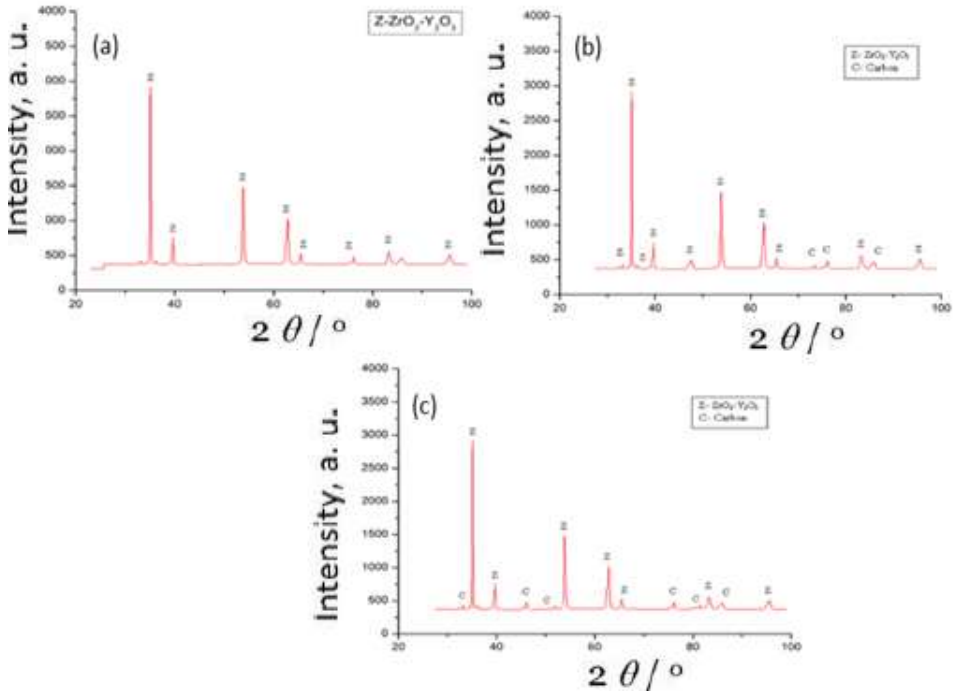

Figure 4. *XRD profile of plasma sprayed: (a) conventional ZrO_2-Y_2O_3; (b) ZrO_2-Y_2O_3 and 1 wt.% CNT; (c) ZrO_2-Y_2O_3 and 4 wt.% CNT coated specimen*

SEM micrographs with EDAX analysis of plasma-sprayed ZrO_2-Y_2O_3, ZrO_2-Y_2O_3 and 1 wt.% CNT and ZrO_2-Y_2O_3 and 4 wt.% CNT coatings on T-91 boiler steel are shown in Figures 5(a)-(c). The coatings consist of interlocked particles having regular morphology with dense structure, as shown in SEM images.

The SEM micrographs shown in Figures 5(b) and 5(c) indicate that the reinforcement of CNT in the coating powders forms a uniform coalescence of ZrO_2-Y_2O_3 and CNT. EDAX analysis confirms the uniform dispersion of CNT in zirconia coating mixtures. Plasma sprayed CNT reinforced coatings over T-91 steel formulate lamellar and dense coating microstructures. EDAX results show the rich presence of Zr with O and some minor percentile of carbon in CNT-reinforced coatings. The

propositions of Zr, O and C in ceramic coatings are nearly approaching the composition of the blended powders used for coating deposition.

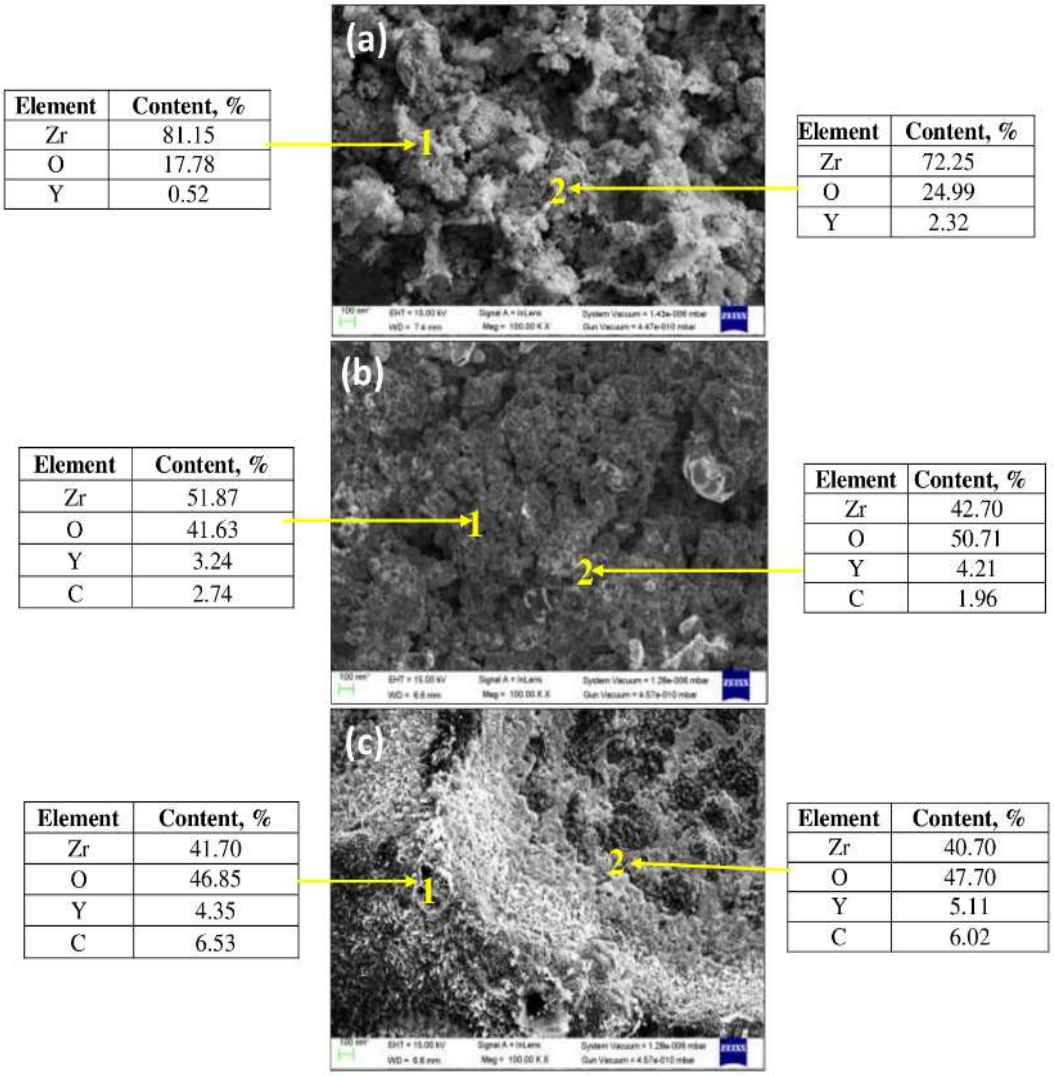

Element	Content, %
Zr	81.15
O	17.78
Y	0.52

Element	Content, %
Zr	72.25
O	24.99
Y	2.32

Element	Content, %
Zr	51.87
O	41.63
Y	3.24
C	2.74

Element	Content, %
Zr	42.70
O	50.71
Y	4.21
C	1.96

Element	Content, %
Zr	41.70
O	46.85
Y	4.35
C	6.53

Element	Content, %
Zr	40.70
O	47.70
Y	5.11
C	6.02

Figure 5. *SEM/EDAX of: (a) conventional ZrO_2-Y_2O_3; (b) ZrO_2-Y_2O_3 and 1 wt.% CNT; (c) ZrO_2-Y_2O_3 and 4 wt.% CNT reinforced composite coatings*

Cross-sectional morphology

The plasma spray conventional and CNT-reinforced samples were examined for cross-sectional morphology with the variation of elemental composition at different points, as shown in Figures 6(a)-(c). Due to the solidification and de-solidification of the molten droplet on the surface of the substrate, steel splat-type morphology can be visualized.

The elemental analysis indicates the presence of Fe content in the substrate of coated specimens. With the reinforcement of CNT in the composite coatings, the traces of carbon content appear and the coatings show a rich percentage of zirconium, yttrium and oxygen. The content of zirconium, yttrium and oxygen were found uniform throughout the surface area, showing that all the composite coatings are uniform in elemental composition.

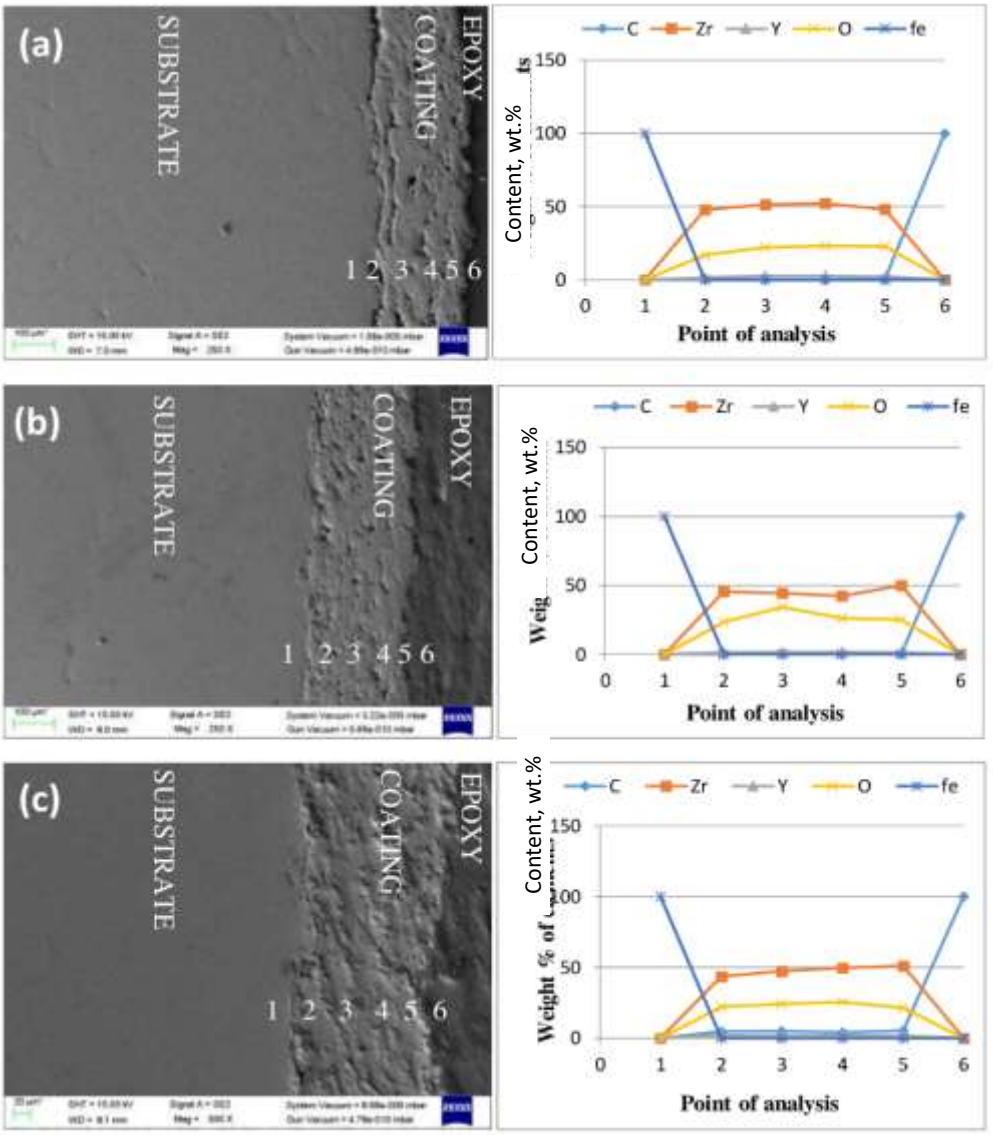

Figure 6. Cross-sectional morphology and the elemental composition of: (a) conventional ZrO_2-Y_2O_3; (b) ZrO_2-Y_2O_3 and 1 wt.% CNT; (c) ZrO_2-Y_2O_3 and 4 wt.% CNT coatings

Elemental X-ray mapping

The ZrO_2-Y_2O_3 and CNT-based ZrO_2-Y_2O_3 composite coatings have been analyzed using the elemental X-ray mapping technique as shown in Figure 7, Figure 8 and Figure 9. In the elemental analysis of the substrate part of all specimens show the rich presence of iron while the reinforced-CNT based coating matrix of specimens shows the presence of zirconium in rich dominance in all X-ray mapping along with the minor presence of carbon as shown in Figure 8 and Figure 9.

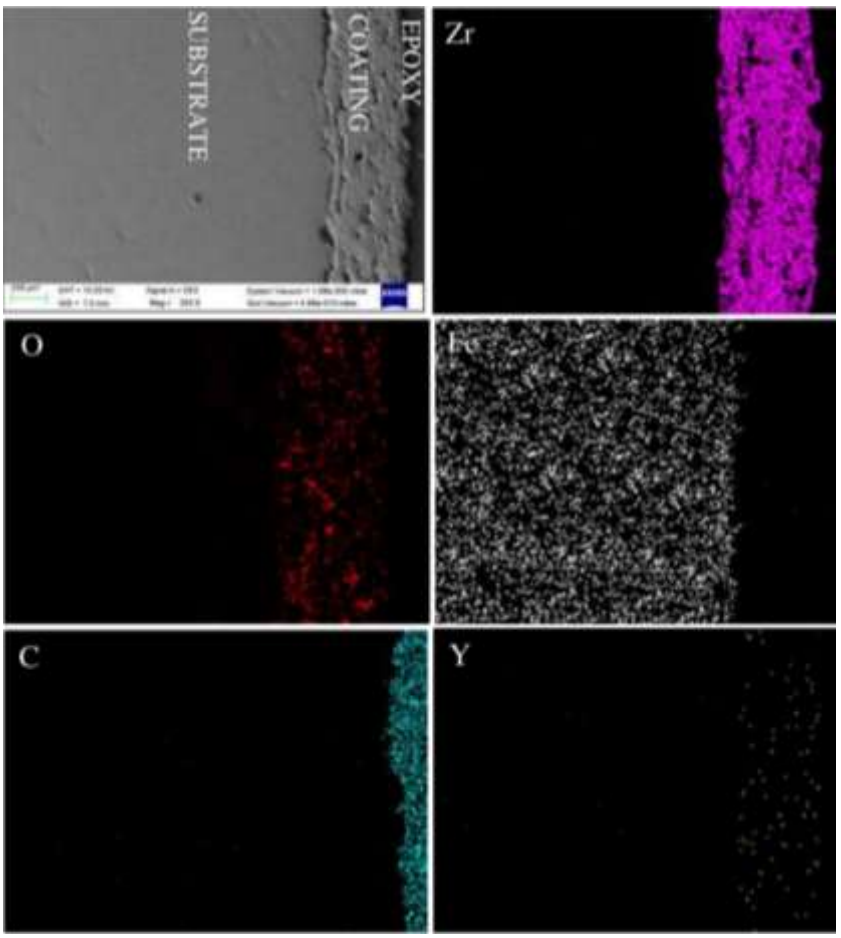

Figure 7. *X-ray mapping along the cross-sectional of conventional ZrO_2-Y_2O_3 coating*

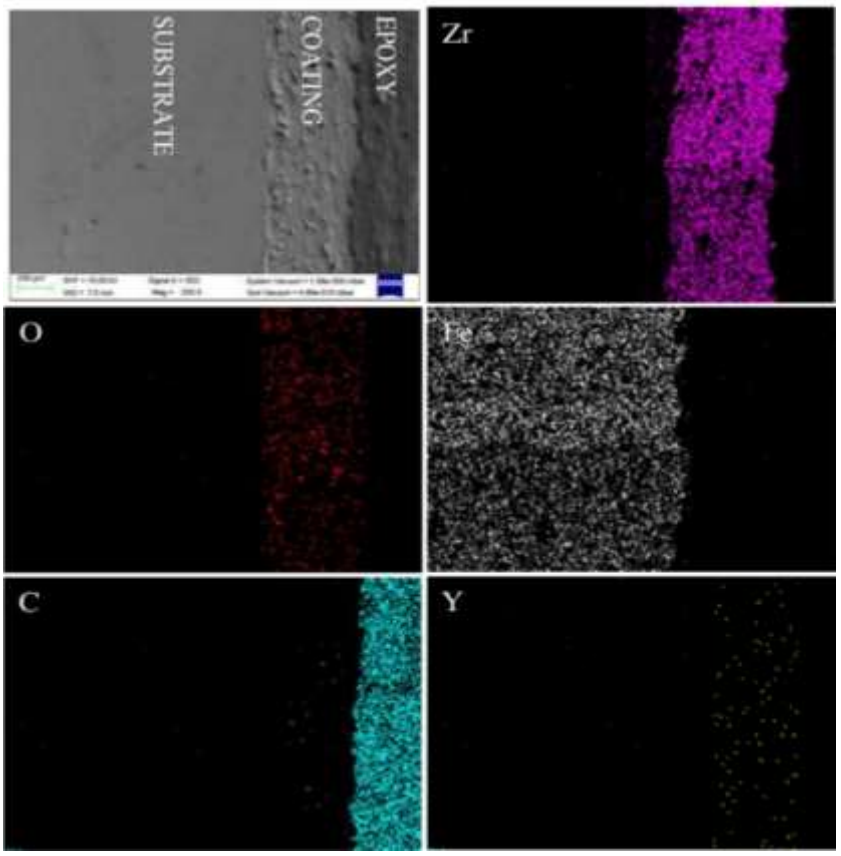

Figure 8. *X-ray mapping along the cross-sectional of ZrO_2-Y_2O_3 and 1 wt.% CNT coating*

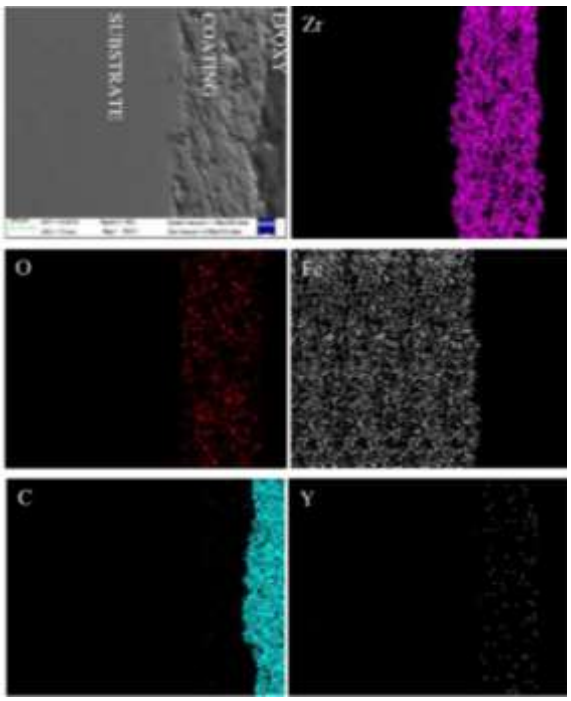

Figure 9. *X-ray mapping along the cross-sectional of ZrO_2-Y_2O_3 and 4 wt.% CNT coating*

Discussion

The coating thickness of all samples was measured along the cross-section of coated specimens. The range of coating thickness was between 250- 270 µm and was uniform throughout the surface. The coating thickness was in the desired range as reported in the literature for plasma spray coatings. In conventional ZrO_2-Y_2O_3 coating deposited over T-91 boiler tube steel, the porosity was found to be 4.25 percent which decreased with the addition of CNT in the ZrO_2-Y_2O_3 composite matrix.

The CNTs were able to lower the porosity of conventional ZrO_2-Y_2O_3 coating. The plasma-sprayed CNT formed a locked structure with ZrO_2-Y_2O_3 grains. The CNTs were able to fill the pores, which helped to decrease the porosity of the ZrO_2-Y_2O_3 composite coating. There is a notable decrease in the value of porosity with an increase in the content of CNT content [16,34,35]. The microhardness values of conventional ZrO_2-Y_2O_3 coated T-91 steel specimen was in the range of 789-796 Hv, as presented in Figure 3. With the addition of CNT in the ZrO_2-Y_2O_3 composite matrix, the microhardness increased tremendously and was between 908-910 Hv for ZrO_2-Y_2O_3 and 1 wt.% CNT coated T-91 specimen and 1047-1051 Hv for ZrO_2-Y_2O_3 and 4 wt.% CNT coated T-91 specimen, respectively. The increase in microhardness results in enhancement in melting point and resistance to indentation [27,36,37]. The increase in microhardness results from CNT presence in the coating powder, which undergoes dispersion hardening. The improvement in microhardness of composite coating acknowledges the main role of CNT reinforcement [38]. ZrO_2-Y_2O_3 was the main phase identified by X-ray diffraction analysis of the ZrO_2-Y_2O_3 coated T-91 boiler steel specimen. The presence of carbon as small peaks in the CNT-based ZrO_2-Y_2O_3 coated specimens proves the presence of pure carbon in the form of CNT. This reveals that CNTs were inert during the spraying and deposition process and have not chemically reacted with the zirconium and yttrium even at high temperatures of plasma spray during the coating process. The presence of carbon content in the X-ray diffraction graphs increases with the increase in the weight percent of CNT in the ZrO_2-Y_2O_3 composite matrix. With the plasma spray process, the composite coatings on substrate T-91 boiler steel material solidify faster. This results in the formation of metastable phases, as presented in X-ray diffraction graphs. Similar findings were reported by researchers in their research work [28,39,40]. The results observed by

SEM/EDAX analysis of conventional ZrO_2-Y_2O_3, ZrO_2-Y_2O_3 and 1 wt.% CNT and ZrO_2-Y_2O_3 and 4 wt.% CNT coated on T-91 boiler steel revealed that the coating is uniform and dense throughout the cross-section. CNT was completely coalescent with the ZrO_2-Y_2O_3 matrix in the composite coating. EDAX analysis at selected points reveals the presence of zirconium, yttrium and oxygen, along with carbon in CNT reinforced coating matrix. As the weight percentage of CNT in ZrO_2-Y_2O_3 coatings increases, the carbon content traces also increase. CNTs form bridge-like stricture between coating matrix [28,39,41]. The results for cross-sectional morphology for CNT-based ZrO_2-Y_2O_3 composite coated T-91 specimens show a completely uniform and dense microstructure of coatings. There seems to be no gap between the interface of substrate and coating layer, which forms strong adhesion due to the good thermal properties of CNT [15]. The results shown by X-ray mapping help to identify the distribution of elements in coating throughout the cross-section. The mapping shows that Fe was present in a rich percentage in the substrate zone. Further coating zone of conventional ZrO_2-Y_2O_3 indicates the presence Zr, Y and O, whereas CNT-based ZrO_2-Y_2O_3 composite coatings show the presence of Zr, Y, O and C, which indicates the presence of CNT in the coating matrix.

Conclusions

The following conclusions are made from this experimental work:

- In the present research work, conventional ZrO_2-Y_2O_3 and CNT reinforced coatings having ZrO_2-Y_2O_3 and 1 wt.% CNT and ZrO_2-Y_2O_3 and 4 wt.% CNT coating were successfully deposited on T-91 boiler tube steel.
- The coating formed had dense and uniform microstructure with coating thickness ranging from 250-270 µm.
- The porosity of the coatings decreased with the increase in CNT weight percentage in the zirconium yttrium matrix, whereas the microhardness of the coatings increased with the addition of CNTs.
- The microhardness of 4 wt.% of CNT reinforcement coated specimen was recorded between 1047-1051 Hv. Due to the strong bond between ZrO_2-Y_2O_3 and CNT, the mechanical properties were improved.
- Scanning electron microscopy morphology shows a uniform distribution of CNT with ZrO_2-Y_2O_3 on T-91 substrate by the plasma spray process. Even at the high temperature of the plasma spray process, CNT was chemically stable and did not react with zirconium and yttrium. The traces of Zr, Y, O and C were shown in EDAX analysis, confirming the presence of major elements in the composite coatings.

References

[1] M. Esfandiari, H. Dong, *Surface and Coatings Technology* **202(3)** (2007) 466-478. https://doi.org/10.1016/j.surfcoat.2007.06.069
[2] R. A. Rapp, *Corrosion Science* **44(2)** (2002) 209-221. https://doi.org/10.1016/S0010-38X(01)00057-9
[3] D. Sapundjiev, *Corrosion Science* **48(3)** (2006) 577-594. https://doi.org/10.1016/j.corsci.2005.04.001
[4] R. Sivakumar, S. V. Joshi, *Transactions of Indian Ceramic Society* **50(1)** (1991) 1-14. https://doi.org/10.1080/0371750X.1991.10804475
[5] H. Zhang, H. Lua, Y. Zhu, F. Li, R. Duan, M. Zhang, X. Wang, *Powder Technology* **227** (2012) 9-16. https://doi.org/10.1016/j.powtec.2012.02.007

[6] B. Bhushan, B. K. Gupta, Handbook of Tribology: Materials, Coatings, and Surface Treatments McGraw-Hill, New York (1991) 259. https://www.osti.gov/biblio/441774
[7] K. Szyma, A. Hernas, G. Moskal, H. Myalska, *Surface and Coatings Technology* **268** (2015) 153-164. https://doi.org/10.1016/j.surfcoat.2014.10.046
[8] N. Kahraman, B. Gülenc, *Materials & Design* **23(8)** (2002) 721-725. https://doi.org/10.1016/S0261-3069(02)00075-4
[9] H. S. Sidhu, B. S. Sidhu, S. Prakash, *Journal of Materials Processing Technology* **171(1)** (2006) 77-82. https://doi.org/10.1016/j.jmatprotec.2005.06.058
[10] S. Deshpande, A. Kulkarni, S. Sampath, H. Herman, *Surface and coatings Technology,* **187(1)** (2004) 6-16. https://doi.org/10.1016/j.surfcoat.2004.01.032
[11] S. Kamal, R. Jayaganthan, S. Prakash, *Surface Coatings Technology* **203(8)** (2009) 1004-1013 https://doi.org/10.1016/j.surfcoat.2008.09.031
[12] S. Iijima, *Nature* **354** (1991) 56-58. https://doi.org/10.1038/354056a0
[13] R. S. Ruoff, D. C. Lorents, *Carbon* **33(7)** (1995) 925-930. https://doi.org/10.1016/0008-6223(95)00021-5
[14] M. S. Dresselhaus, G. Dresselhaus, P. C. Eklund, *Sci. Fullerenes Carbon Nanotube* **917** (1996) 870-917. https://doi.org/10.1016/b978-012221820-0/50020-4
[15] M. Sharma, V. Sharma, *International Journal of Minerals, Metallurgy, and Materials* **23(2)** (2016) 222-233. https://doi.org/10.1007/s12613-016-1230-3
[16] K. Goyal, H. Singh, R. Bhatia, *Advanced Engineering Forum* **26** (2018) 53-66. https://doi.org/10.4028/www.scientific.net/AEF.26.53
[17] E. T. Thostenson, C. Li, T. W. Chou, C*omposites Science and Technology* **65(3)** (2005) 491-516. https://doi.org/10.1016/j.compscitech.2004.11.003
[18] C. F. Deng, D. Z. Wang, X. X. Zhang, A. B. Li, *Materials Science and Engineering A* **444(1)** (2007)138-145. https://doi.org/10.1016/j.msea.2006.08.057
[19] M. K. Singla, H. Singh, V. Chawla, *Journal of Minerals and Materials Characterization and Engineering* **10(8)** (2011) 717-726.
[20] B. M. Praveen, T. V Venkatesha, Y. A. Naik, K. Prashantha, *Surface and Coatings Technology* **201(12)** (2007) 5836-5842. https://doi.org/10.1016/j.surfcoat.2006.10.034
[21] K. Balani, S. P. Harimkar, A. Keshri, Y. Chen, N. B. Dahotre, A. Agarwal, *Acta Materialia* **56(20)** 5984-5994. https://doi.org/10.1016/j.actamat.2008.08.020
[22] I. Ahmad, M. Unwin, H. Cao, H. Chen, H. Zhao, A. Kennedy, Y. Q. Zhu, *Composites and Science Technology* **70(8)** (2010) 1199-1206. https://doi.org/10.1016/j.compscitech.2010.03.007
[23] A. K. Keshri, V. Singh, J. Huang, S. Seal, W. Choi, A. Agarwal, *Surface and Coatings Technology* **204(11)** (2010) 1847-1855. https://doi.org/10.1016/j.surfcoat.2009.11.032
[24] M. O. Bodunrin, K. K. Alaneme, L. H. Chown, *Journal of Materials Research and Technology* **4(4)** (2015) 434-445. https://doi.org/10.1016/j.jmrt.2015.05.003
[25] C. F. Gutierrez-Gonzalez, A. Smirnov, A. Centeno, A. Fernández, B. Alonso, V. G. Rocha, R. Torrecillas, A. Zurutuza, J. F. Bartolome, *Ceramics International* **41(6)** (2015) 7434-7438. https://doi.org/10.1016/j.ceramint.2015.02.061
[26] K. Goyal, *World Journal of Engineering* **15(4)** (2018) 429-439. https://doi.or/10.1108/WJE-10-2017-0315
[27] H. Chen, X. Zhou, C. Ding, *Journal of the European Ceramic Society* **23(9)** (2003) 1449-1455. https://doi.org/10.1016/S0955-2219(02)00345-X
[28] K. Goyal, H. Singh, and R. Bhatia, *Journal of the Australian Ceramic Society* **55(2)** (2019) 315-322. https://doi.org/10.1007/s41779-018-0237-9
[29] B. S. Sidhu, D. Puri, S. Prakash, *Journal of Materials Processing Technology* **159(3)** (2005) 347-355. https://doi.org/10.1016/j.jmatprotec.2004.05.023

[30] K. Katiki, S. Yadlapati, S. N. S. Chidepudi, P. R. Hari, *International Journal of ChemTech Research* **6(11)** (2014) 4579-4584. https://www.sphinxsai.com/2014/ch_vol6_no11/1/(4579-4584)N14.pdf
[31] J. Mehta, V. K. Mittal, and P. Gupta, *Journal of Applied Science and Engineering* **20(4)** (2017) 445-452. https://doi.org/10.6180/jase.2017.20.4.05
[32] S. S. Chatha, H. S. Sidhu, B. S. Sidhu, *Journal of Minerals & Materials Characterization & Engineering* **11(06)** (2012) 569-586. https://doi.org/10.4236/jmmce.2012.116041
[33] P.-H. Gao, Y.-G. Li, C.-J. Li, G.-J. Yang, C.-X. Li, *Journal of Thermal Spray Technology* **17** (2008) 742-749. https://doi.org/10.1007/s11666-008-9258-1
[34] A. Pathak, S. Mathiyalagam, K. K. Pandey, P. Bijalwan, M. Dutta, A. K. Keshri, *International Journal of Applied Ceramic Technology* **16(6)** (2019) 2306-2315. https://doi.org/10.1111/ijac.13327
[35] W. Guo, H. Y. Tam, *The International Journal of Advanced Manufacturing Technology* **72** (2014) 269-275. https://doi.org/10.1007/s00170-014-5661-6
[36] J. Ning, J. Zhang, Y. Pan, J. Guo, *Materials Science and Engineering A* **357(1–2)** (2003) 392-396. https://doi.org/10.1016/S0921-5093(03)00256-9
[37] E. Edward Anand, S. Natarajan, *Journal of Materials Engineering and Performance* **24(1)** (2015) 128-135. https://doi.org/10.1007/s11665-014-1306-z
[38] P. R. Silva, V. O. Almeida, G. B. MacHado, E. V. Benvenutti, T. M. H. Costa, M. R. Gallas, *Langmuir* **28(2)** (2012) 1447-1452. https://doi.org/10.1021/la203056f
[39] A. K. Keshri, A. Agarwal, *Surface and Coatings Technology* **206(2-3)** (2011) 338-347. https://doi.org/10.1016/j.surfcoat.2011.07.025
[40] B. Singh, D. Puri, S. Prakash, *Journal of Materials Processing Technology* **159(3)** (2005) 347-355. https://doi.org/10.1016/j.jmatprotec.2004.05.023
[41] C. F. Deng, D. Z. Wang, X. X. Zhang, A. B. Li, *Materials Science and Engineering A* **444(1-2)** (2007) 138-145. https://doi.org/10.1016/j.msea.2006.08.057